Theoretical and Applied Fracture Mechanics 120 (2022) 103404

Contents lists available at ScienceDirect

Theoretical and Applied Fracture Mechanics

journal homepage: www.elsevier.com/locate/tafmec

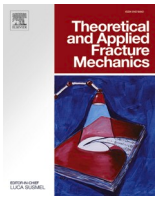

Fracture characterisation of bone-cement bonded joints under mode I loading

T.D. Campos [a,b], M.L.S. Barbosa [c], A.A.R. Olmos [a,b], M. Martins [a,b], F.A.M. Pereira [d], M.F.S.F. de Moura [e], A. Zille [f], N. Dourado [a,b,*]

[a] CMEMS-UMINHO, Universidade do Minho, 4800-058 Guimarães, Portugal
[b] LABBELS –Associate Laboratory, Braga, Guimarães, Portugal
[c] Instituto Politécnico do Porto, Instituto Superior de Engenharia do Porto, 4200-072, Portugal
[d] CITAB/UTAD, Departamento de Engenharias, Quinta de Prados, 5001-801 Vila Real, Portugal
[e] Faculdade de Engenharia, Dep. de Eng. Mecânica, Universidade do Porto, Portugal
[f] 2C2T-Centro de Ciência e Tecnologia Têxtil, Universidade do Minho, Portugal

ARTICLE INFO

Keywords:
Cortical bone tissue
Bone fracture
Bone cement
Cohesive Zone Modelling
Finite element modelling

ABSTRACT

Over the years, many techniques have been developed for the stabilisation of bone fractures. The study of the adhesion of bone-to-bone cement is an important step towards the development of new immobilization systems. Although bone cement has been used for more than fifty years, very few studies have been performed regarding the evaluation of fracture properties. In this work, numerical and experimental investigations were conducted to evaluate the strain energy release rate under mode I loading in a bone-cement bonded joint, using the Double Cantilever Beam (DCB) test. Cohesive zone laws were also measured combining the finite element method with non-linear elastic fracture mechanics. This has been made in a cortical bone bonded joint with polymethylmethacrylate (PMMA). Consistent results have been obtained regarding fracture toughness in a widely used bone-to-bone cement joint in many biomedical applications.

1. Introduction

Cortical bone is considered as a quasi-brittle material presenting a complex, anisotropic, hierarchical, and heterogeneous microstructure, with high ability to fracture [1–3]. The structural integrity, porosity, organisation, and physical–chemical constitution of bone, directly influence the evolution of the bone tissue failure process [2,3]. Predictions of fracture growth, as well as stress and displacement fields are possible to obtain, by combining the Finite Element Method (FEM) with Cohesive Zone Models (CZM), providing that suitable failure criteria are used. In fact, CZM are particularly adequate to deal with quasi-brittle materials characterised by the existence of a non-negligible fracture process zone. Norman et al. [4] considered the concepts of this technique and performed fracture analyses of human and bovine bones using the Compact Tension (CT) test. Yang et al. [5] tested humerus cortical bone also with the CT test and considered two different approaches: linear elastic fracture mechanics (LEFM) and nonlinear fracture mechanics (NLFM) considering a CZM. The authors observed that the LEFM was unable to mimic load–displacement curves, but the NLFM was able to predict several load–displacement curves after calibration with data from one curve. Thus, the authors state that LEFM is not an accurate model to be applied to cortical bone tissue and the nonlinear CZM is a more accurate approach to predict bone fracture behaviour. Morais et al. [6] used a miniaturised version of the Double Cantilever Beam (DCB) test to undergo fracture characterisation of cortical bone tissue under opening mode. The authors refer that the DCB test allows a more stable crack growth, providing adequate conditions for an unrestrained development of the fracture process zone (i.e., self-similar crack propagation). They considered NLFM approach through numerical simulation, incorporating CZM and determined the corresponding *Resistance*-curves. Pereira et al. [7] used the DCB test to determine the representative cohesive laws of fracture in hydrated and dehydrated bovine cortical bone tissue to evaluate the influence of water content on cohesive laws and fracture toughness. These authors employed an inverse method based on a genetic algorithm and pointed out the changes in the ductility of the material and consequent effects in the fracture mechanisms as a function of

* Corresponding author at: CMEMS-UMINHO, Universidade do Minho, 4800-058 Guimarães, Portugal.
E-mail addresses: teresa.ac.biome@gmail.pt (T.D. Campos), andrea.olmos@dem.uminho.pt (A.A.R. Olmos), mmartins@dei.uminho.pt (M. Martins), famp@utad.pt (F.A.M. Pereira), mfmoura@fe.up.pt (M.F.S.F. de Moura), azille@det.uminho.pt (A. Zille), nunodourado@dem.uminho.pt (N. Dourado).

https://doi.org/10.1016/j.tafmec.2022.103404
Received 31 March 2022; Received in revised form 11 May 2022; Accepted 11 May 2022
Available online 17 May 2022

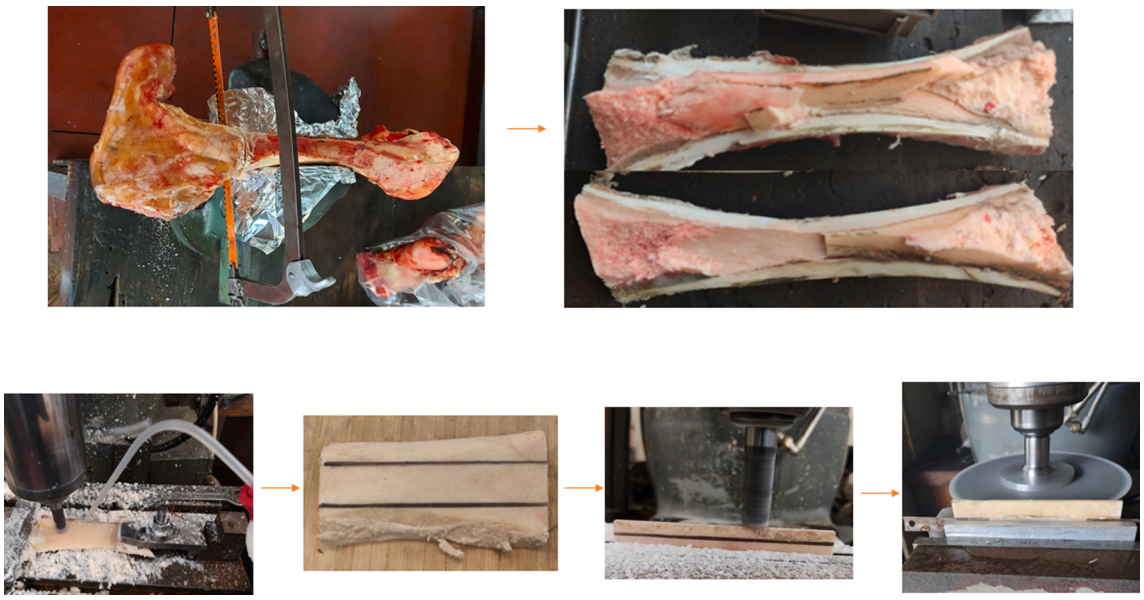

Fig. 1. Manufacturing steps of bone samples.

Fig. 2. Bone cement production process.

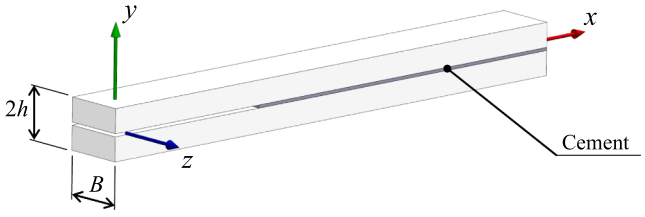

Fig. 3. Schematic representation of the DCB test.

Table 1
Specimen dimensions.

Specimen	2*h* (mm)	*B* (mm)
1	7.8	8.1
2	7.1	6.2
3	9.0	11.0
4	9.4	10.0
5	7.2	7.4
6	5.6	6.8

the hydration of the cortical bone tissue.

Bone fractures decrease the patient's quality of life and entail high costs for the health care system. When a bone fractures, it is imperative to maintain its alignment during the recovery phase in order to ensure its correct healing. In situations where it is not possible to maintain alignment in the face of external fixators (e.g., such as plaster), it

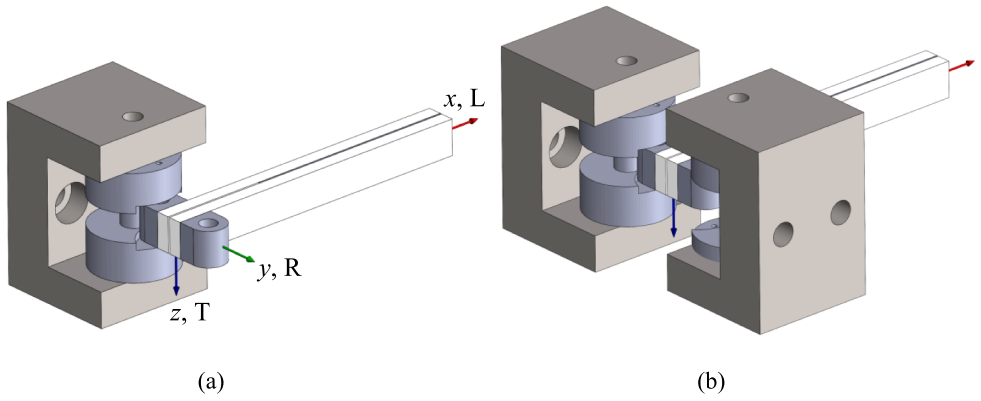

Fig. 4. Setup of DCB test in cement-bone: (a) partially assembled and (b) fully-assembled.

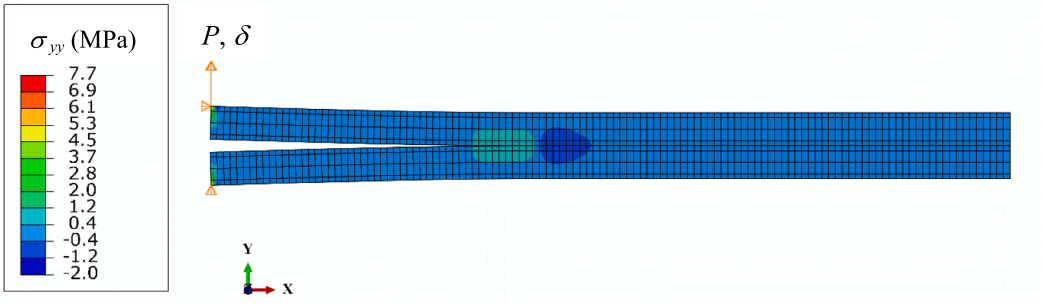

Fig. 5. Modelling of damage initiation and propagation in the DCB test.

Table 2
Fracture properties of bovine cortical bone [18].

E_L (GPa)	E_T (GPa)	G_{LT} (GPa)	ν_{LT}
*	9.55	4.74	0.37

* (*) Obtained for each specimen by an iterative procedure involving FE analysis.

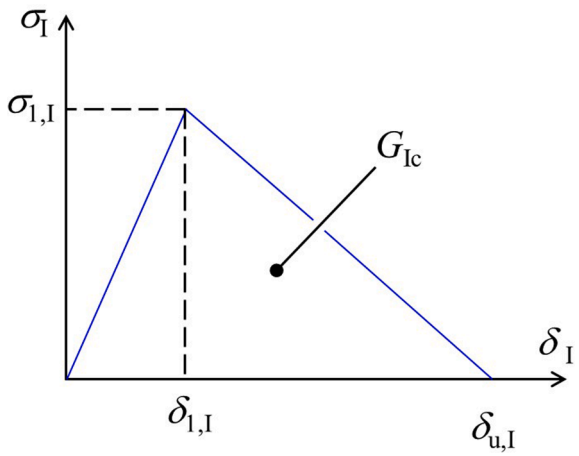

Fig. 6. Bi-linear cohesive law with linear softening relationship.

becomes essential to apply internal fixators; however, conventional internal fixation methods are associated with several clinical problems [8]. As such, the use of other forms of bone stabilisation solutions, ideally non-metallic, could be a colossal asset to aid fracture repair. Examples of non-metallic fixation solutions are fibrous systems (e.g., impregnated in polymer polyvinyl alcohol, PVA) [9], which may require the employment of bone cement as the binding material to bone. Numerous solutions could be developed using hydrophilic water-soluble synthetic polymer polyvinyl alcohol (PVA) in a fibrous form if its mechanical behaviour (both monotonic and viscoelastic) was sufficiently known. Several types of adhesives have been used in the fixation of implants in orthopaedic and traumatic surgeries. Polymethylmethacrylate (PMMA) is the main constituent of the most widely used bone cement nowadays [10–12]. Bone cement in hip arthroplasties allows sustaining the forces that are transmitted through the hip joint. Debonding, cracking of cement mantle, and loosening of cemented hip arthroplasties can originate serious complications requiring revision surgery [13]. In this context, the study of the bone-cement bonded joints considering bone as the substrate becomes relevant. The literature reports the application of the LEFM approach [14–15] to analyse the influence of crack at the implant-cement interface on failure. The Mann and Bhashyam (1999) [14] study consisted of determining the fracture toughness of the cobalt-chromium/polymethylmethacrylate bond under mixed-mode loading conditions. For this, they combined finite element analyses and experimental fracture mechanics tests. Also, Mann (2001) [15] studied the mechanical behaviour of the cement-bone interface under mixed-mode loading (combined tensile and shear stresses) in order to develop a failure model. These results allow the determination of the onset and progression of interface failure in cemented total hip replacements. On the other hand, several authors have adopted the NLFM concepts to characterise bone [6–7] and cement-bone joints [13,16], due to non-negligible fracture process zone. Wang et al. (2000) [16] employed a bone-cement interface compact sandwich (BCS) specimen to estimate interfacial fracture toughness under pure mode I loading. The authors performed finite element analysis (FEA) to investigate the effect of the interlayer thickness, considering bone as an isotropic material. The mode mixity at the crack tip is primarily affected by the material mismatch and interlayer thickness, in the BCS

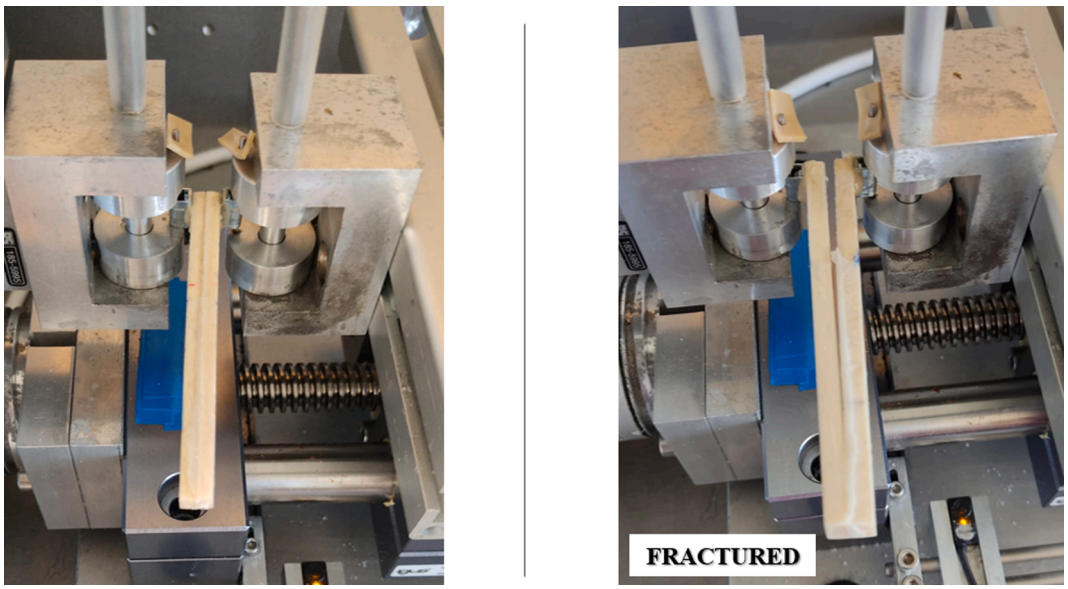

Fig. 7. Experimental setup of the DCB test.

specimens. The researchers concluded that there are many factors capable of significantly affect the measurement of interfacial fracture toughness. The material mismatch at the interface and the thickness of the intermediate layer are described as the most important. Intensity variations at the crack tip induce fracture toughness to be underestimated or overestimated [16].

Taking into account the well-succeed procedures regarding bone fracture characterisation under mode I loading using the DCB test [6], it was decided to employ a similar strategy to bone-cement bonded joints. Hence, in this study bone-cement bonded joints were manufactured with DCB configuration for quasi-static pure mode I fracture characterisation. *Resistance*-curves (*R*-curves) were evaluated using the Compliance-Based Beam Method (CBBM). An inverse method was adopted combining the Finite Element Method and experimental data to identify cohesive laws, which allows mimicking damage initiation and propagation in the adhesive layer. The developed procedure rendered possible to determine the critical strain energy release rate of bone-cement bonded joint.

2. Experimental work

2.1. Preparation of biological samples

Samples of cortical bone extracted from femurs of 6 fresh adult bovines following euthanasia were prepared (Fig. 1). The specimens were harvested from the internal medial area of the femoral diaphysis (bone region of higher stiffness) of long bones. The preparation of the referred specimens was executed through cutting and machining processes following both acetic and safety standards. Cutting operations consisted of removing the proximal epiphysis, followed by a cut along the longitudinal direction with the purpose of splitting the diaphysis into two halves without bone marrow. The machining operations were executed in a milling equipment to obtain parallelepiped samples, using a 16 mm diameter end mill (Sandvik Coromant® ref. R216.34–16050) with an angular frequency of 3000 rpm. A ceramic disk (0.8 mm thick; BUEHLER® ref. 111190) was used to cut horizontally the bone tissue to obtain bone samples with a considerable length. Following these procedures, bone samples were wrapped in gauzes duly moistened with saline solution and then frozen at −20 °C.

2.2. Preparation of bone cement

Polymethylmethacrylate (PMMA) cement (DePuy® Synthes | J&J Company ref. CMW 3) was provided in a powder base and as a liquid monomer (Fig. 2). PMMA-cement was prepared according to DePuy® datasheet instructions. Both components were mixed homogeneously to avoid the formation of pores, thus obtaining a mass with proper viscosity.

2.3. Preparation of bonded joint

Specimens were produced bonding two arms harvested from the same femur. Polymethylmethacrylate (PMMA) bone-cement was smeared over the surface of one arm and subsequently pressed against the other arm (Fig. 3). A Teflon® foil was used (thickness 0.2 mm) between both specimen arms to guarantee the adhesive thickness. Bone cement was applied to one arm and then joined to the second one, keeping the union under pressure (Fig. 3). The adhesive cure was then made at room temperature for 3 days. Two blocks of aluminium-alloy were fixed to the specimen arms using Araldite® 2015 to allow load application (Fig. 4(a)).

In Table 1 the dimensions of each specimen subjected to DCB tests are presented. An initial crack length (a_0) equal 30 mm was defined for each specimen.

2.4. Mechanical tests

DCB tests were executed in a servo-hydraulic testing system using a 50 N load-cell to obtain load–displacement curves (P–δ curves). Specimens were loaded in adequate environmental laboratorial conditions (65% relative humidity at 20 °C) through pin-hole connections leading to pure mode I loading. The configuration of a DCB test in a bonded joint specimen is shown in Fig. 4(b).

2.5. Data reduction scheme

A data reduction scheme (Compliance Based Beam Method - CBBM) based on Timoshenko beam theory, specimen compliance and crack equivalent concept was used to estimate the evolution of the mode I energy release rate during the test. The compliance ($C = \delta/P$) function is determined considering the Timoshenko beam theory [6],

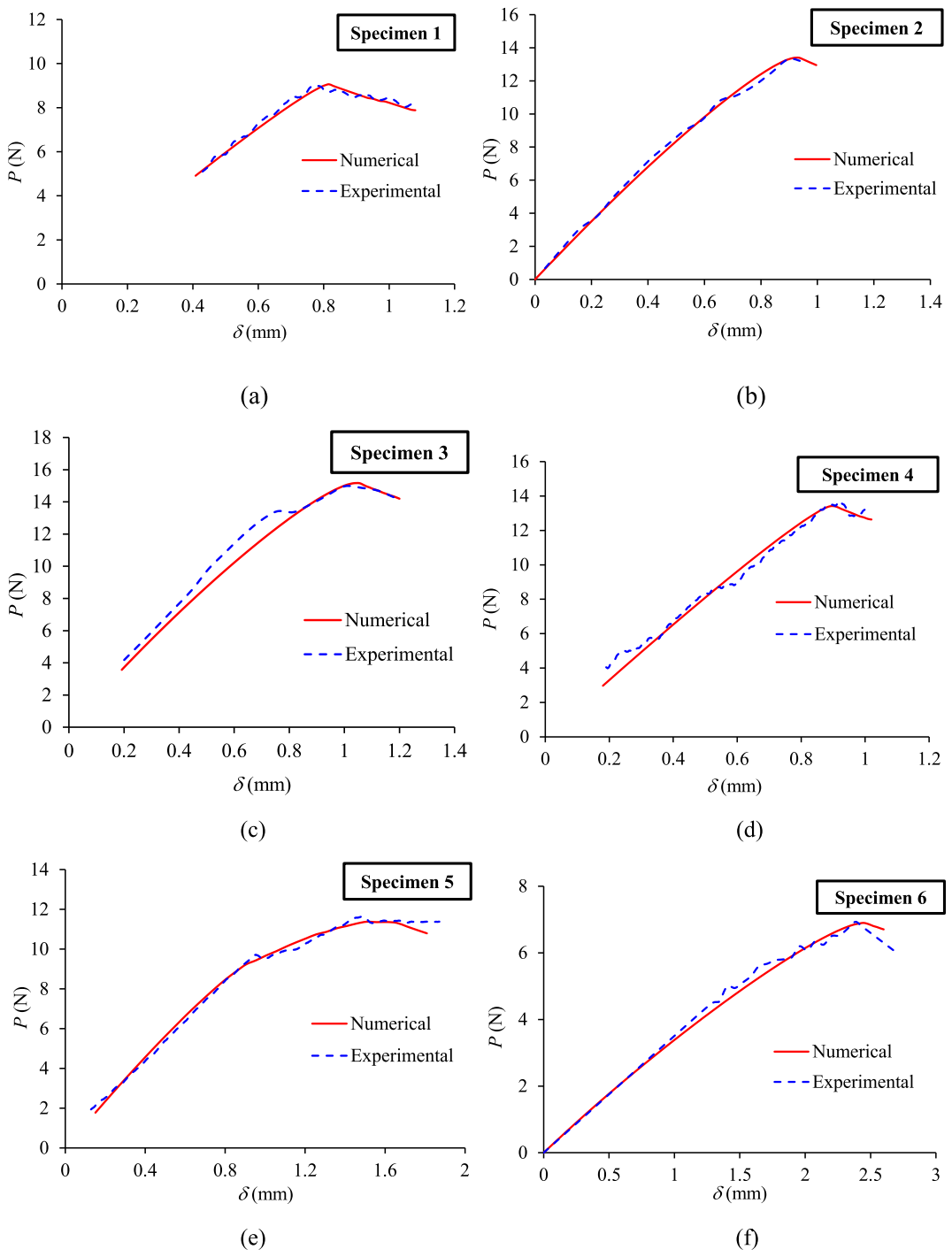

Fig. 8. Experimental and numerical P-δ curves.

$$C = \frac{8a^3}{E_L B h^3} + \frac{12a}{5BhG_{LT}} \tag{1}$$

being E_L the longitudinal elastic modulus, G_{LT} the shear modulus in the LT plane (Fig. 4a), and B, h and a are specimen dimensions given in Fig. 3. From this equation, it is possible to obtain the equivalent crack length (a_e) as a function of the current specimen compliance C obtained through the measured load–displacement (P–δ) curve. The longitudinal modulus of each specimen E_L was estimated by a numerical iterative procedure aiming to fit the numerical initial compliance prior to damage onset (C_0) to the experimental one. The problem of non-negligible scatter of elastic properties in cortical bone is thus overcome, since the elastic modulus is duly captured using this procedure. Combining the Irwin–Kies relation,

$$G_I = \frac{P^2}{2B}\frac{dC}{da} \tag{2}$$

with Eq. (1), where a is replaced by a_e, yields,

$$G_I = \frac{6P^2}{B^2 h}\left(\frac{2a_e^2}{E_L h^2} + \frac{1}{5G_{LT}}\right) \tag{3}$$

This relation is used to plot the R-curve (i.e., $G_I = f(a_e)$) without the direct measurement of the current crack length (a).

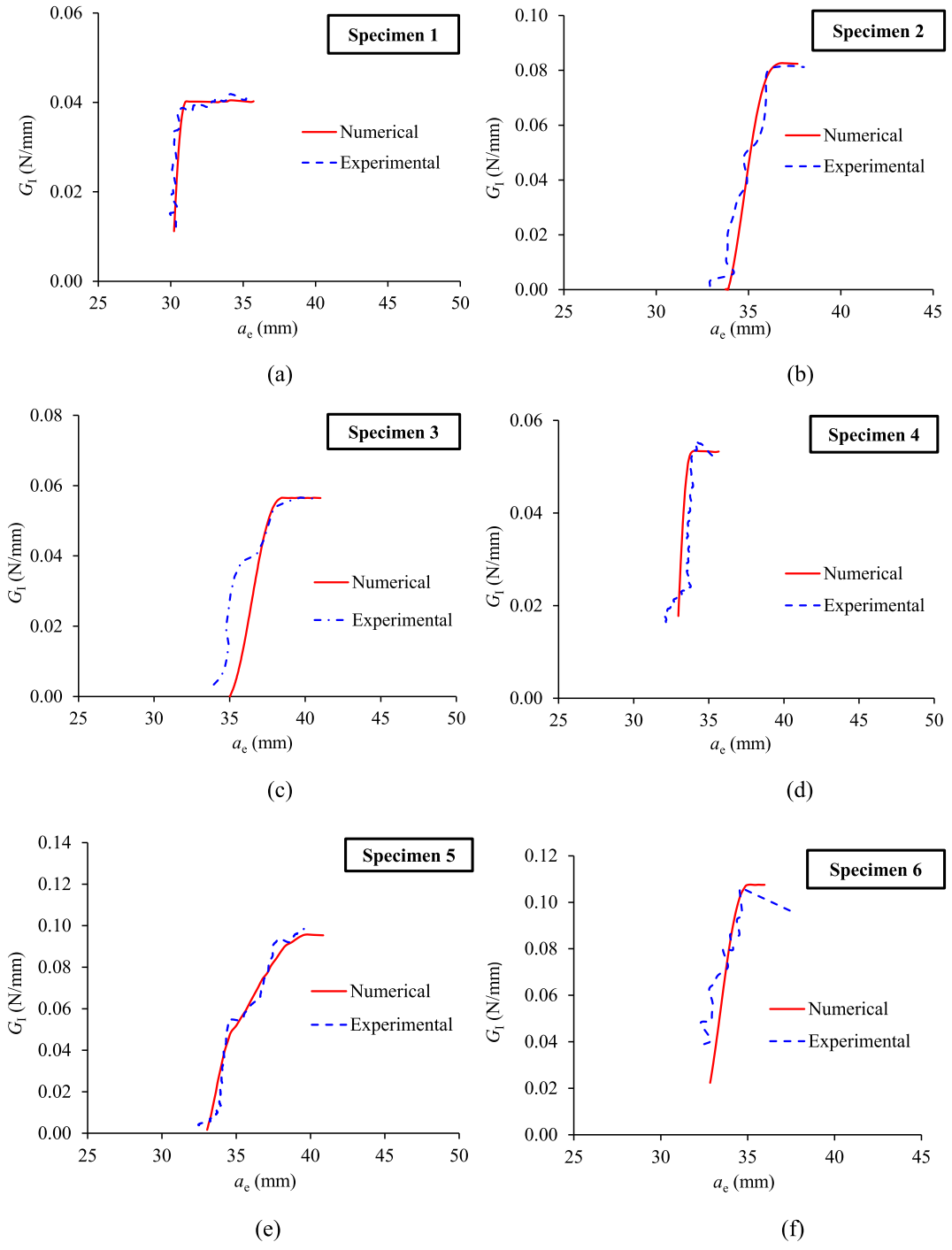

Fig. 9. Experimental and numerical *R*-curves.

Table 3
G_{Ic} values obtained experimentally.

Specimen	G_{Ic} (N/mm)
1	0.040
2	0.082
3	0.060
4	0.053
5	0.100
6	0.107
Average	0.074
CoV (%)	36.53

3. Numerical model

The validation of the proposed data reduction scheme (CBBM) was performed through numerical analysis considering the FEM (ABAQUS® 2021 [17]) including a CZM. This was executed using interface (null-thickness) cohesive elements by means of a developed user-subroutine (Fortran), which allows computing a versatile simulation of damage initiation and growth under different loading conditions. The two-dimensional model is composed of 960 two-dimensional quadratic solid elements (constant width) and 120 compatible interface cohesive elements (with three integration points per element), for a total of 3378 nodes (Fig. 5). A mesh refinement was imposed to allow a stable and

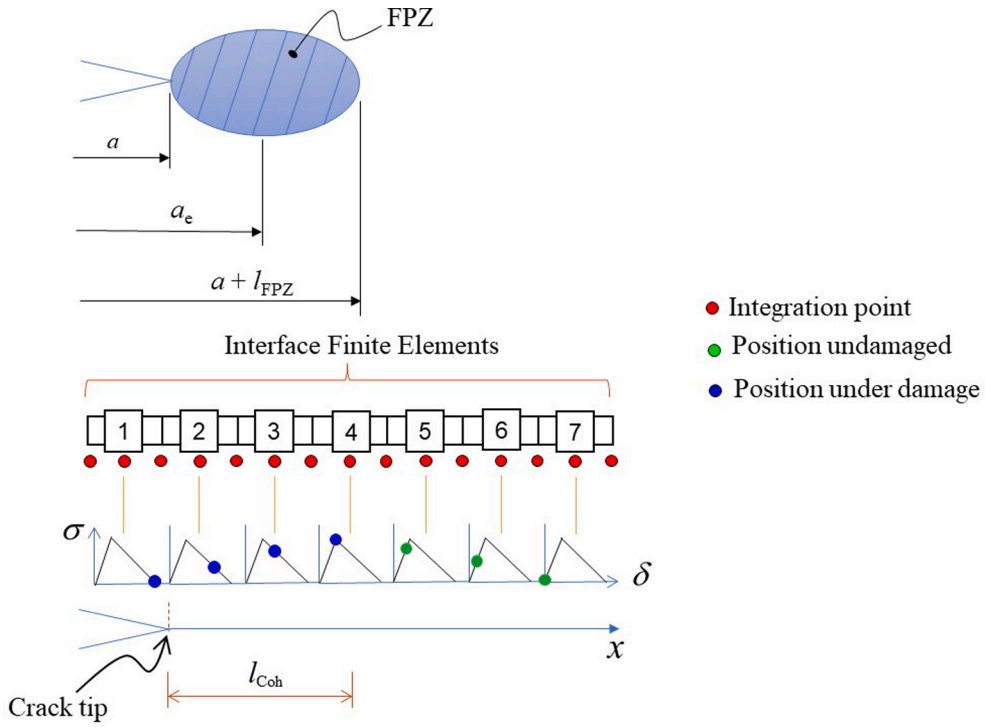

Fig. 10. Representation of the FPZ and the cohesive zone length.

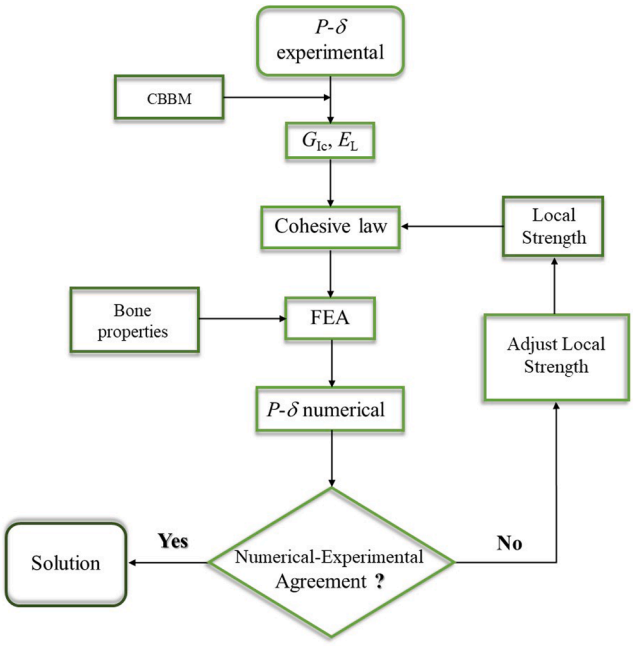

Fig. 11. Schematic representation of the methodology applied to obtain cohesive parameters.

accurate estimation of damage initiation and propagation along the specimen length (longitudinal direction). Loading displacement with small increments (0.01% of total applied displacement) was applied to guarantee smooth propagation.

Bone cement was neglected in the numerical model due to its negligible thickness in comparison to the bone parts. Cortical bone tissue was modelled as a continuous, homogeneous material, transversally isotropic, and with a linear elastic behaviour (Table 2). The analysis was performed under plane stress conditions and assuming a non-linear geometric behaviour.

4. Cohesive zone model

A linear cohesive zone law (Fig. 6) [19,20] was used to simulate damage onset and propagation. A constitutive relationship between the vectors of stresses ($\boldsymbol{\sigma}$) and relative displacements ($\boldsymbol{\delta}$) is established. The method requires the local strength ($\sigma_{u,I}$) and the critical strain energy release rate (G_{Ic}) as inputted data parameters.

In the initial linear branch, the normal tractions (σ_I) are related with the relative displacements (δ_I) by.

$$\sigma_I = k\delta_I \tag{4}$$

where the parameter k represents the normal interface stiffness, which is chosen by the user. This parameter should be as high as possible in order to not interfere with the specimen compliance [21]. Values in the range of 1E6 $\leq k \leq$ 1E7 N/mm^3 generally produce good results. As discussed in [20] very high values of k lead to numerical problems and low values can interfere with the physics of the problem, e.g., interpenetrations between the specimen arms or influence on the specimen compliance. In the present work a value of $k =$ 1E6 N/mm^3 showed a good performance, i.e., no numerical instabilities were observed and specimen compliance was not affected. Following damage initiation (i.e. for $\delta_I \geqslant \delta_{I,I}$), the constitutive law (Eq. (4)) is modified to consider damage onset,

$$\sigma_I = (1-d)k\delta_I \tag{5}$$

where d represents the damage parameter given by,

$$d = \frac{\delta_{u,I}\left(\delta_I - \delta_{I,I}\right)}{\delta_I\left(\delta_{u,I} - \delta_{I,I}\right)} \tag{6}$$

being $\delta_{I,I}$ and $\delta_{u,I}$ the onset and ultimate relative displacements of the softening region, respectively, while δ_I is the current relative displacement. The onset relative displacement $\delta_{I,I}$ is obtained from the local strength and interface stiffness (Eq. (4)), while the ultimate one $\delta_{u,I}$ derives from the mode I fracture energy through the following relation,

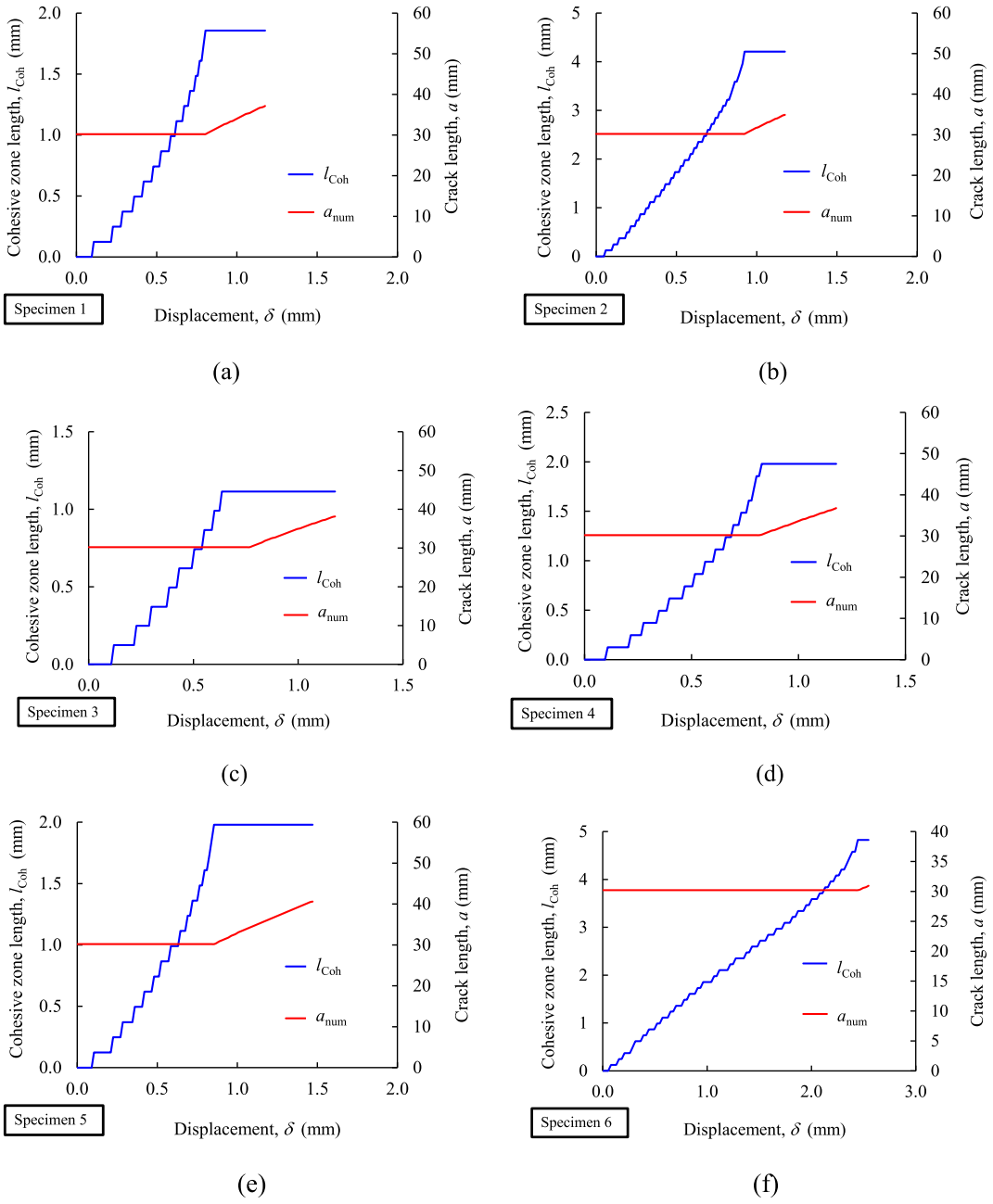

Fig. 12. Development of the cohesive length and corresponding numerical crack extension.

Table 4
Fracture parameters for mode I loading.

Specimen	G_{Ic} (N/mm)	E_L (GPa)	$\sigma_{1,I}$ (MPa)
1	0.040	7.3	7.00
2	0.082	15.5	5.00
3	0.060	7.4	4.00
4	0.053	7.5	8.00
5	0.100	8.5	4.00
6	0.107	6.5	3.00
Average	0.074	8.78	5.17
CoV(%)	36.5	38.2	37.6

$$G_{Ic} = \frac{1}{2}\sigma_{u,I}\delta_{u,I} \tag{7}$$

5. Results and discussion

The CBBM was employed to determine the *R*-curves from the *P*-δ curves resulting from DCB tests on bonded joints of bovine bone and bone cement (Fig. 7). Six valid tests were obtained (Fig. 8) showing a non-negligible non-linear domain following the damage initiation. Cohesive failure occurred in all specimens, i.e., inside the cement. In fact, both DCB specimen fracture surfaces reveal the presence of traces of a thin film of cement. This statement guarantees an almost pure mode I loading owing to symmetrical geometry (rigorous equal specimen arms) and material symmetry (both specimen arms harvested from the same femur).

The CBBM was applied to the experimental *P*-δ curves to determine

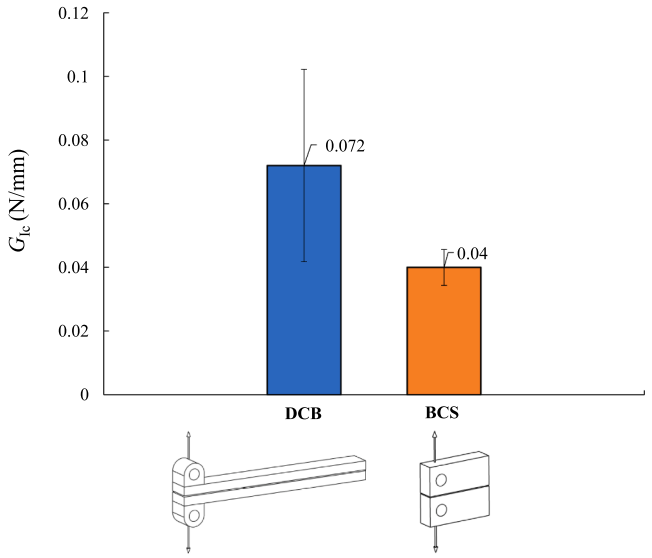

Fig. 13. Values of G_{Ic} ensuing from the DCB and BCS tests [12].

the *R*-curves (Fig. 9). The initial ascending branch of the *R*-curve corresponds to development of the fracture process zone (FPZ). Subsequent to this region, a plateau arises, which demonstrates the development of a so-called self-similar crack growth with constant energy release rate (i.e., the value of G_{Ic}). Table 3 resumes the set of values ensuing from the experiments.

The evaluation of the extension of the cohesive length is an important procedure to verify whether the fracture process zone is fully developed, providing that an adequate numerical agreement has been accomplished. Fig. 10 illustrates the development of the FPZ, together with the crack length. Numerically, the extension of the FPZ is mimicked by the cohesive length (l_{Coh}), which corresponds to the distance between the numerical crack tip and the last integration point of the cohesive element under damage.

Fig. 8 (a)-(f) show the numerical agreement of the *P*-δ curves by means of an inverse method (IM) leading to the identification of the local strength $\sigma_{1,I}$ (Fig. 6) for each specimen. It should be noted that the total area of the cohesive law for mode I loading corresponds to the value of the critical energy release rate (G_{Ic}) determined experimentally. Fig. 11 resumes the procedure adopted in the IM that combines finite element analysis (FEA) with experimental data (*P*-δ curves). The compliance based beam method (CBBM) was also employed to determine the *R*-curves (Fig. 9) ensued from the numerical *P*-δ curves obtained from the IM. It is possible to observe a nice agreement with the experimental data, which is coherent.

Fig. 12 (a)-(f) show the plotting of the numerical crack length (a_{num}), together with the extension of the cohesive zone length (l_{Coh}), as a function of the applied displacement (δ). It is clear that the crack propagation occurs when the extension of the cohesive zone is fully developed. Moreover, the attainment of a critical value ($l_{Coh\ c}$), i.e., a plateau, emphasizes the fulfilment of the condition of self-similar crack propagation. This is a key aspect on the validation of the procedure to determine accurate values ofG_{Ic}. Some variation on the cohesive zone length ($l_{Coh\ c}$) can be noted (Fig. 12), which can be explained by differences of the cohesive parameters (Table 4). In fact, the values of $l_{Coh\ c}$ varies with these parameters (cohesive strength and fracture energy) of the assumed softening law (Fig. 6).

The average value of the critical energy release rate (G_{Ic}) obtained by the CBBM (Table 3) for the DCB test is within the same order of magnitude as the one determined by Wang and Agrawal [11] (see Fig. 13). However, it should be noted that those authors employed the Bilayer Compact Sandwich (BCS) test, which is known to prevent the development of the FPZ due to geometrical constraints. As a consequence, the condition of self-similar crack propagation is not fulfilled in the BCS. Anyway, it is legitimate to undergo such a comparison due to resemblance of the material disposition (i.e., bone-cement-bone).

The values of G_{Ic} estimated experimentally were used as input in the numerical model, together with an inverse procedure, to estimate the longitudinal modulus E_L and the normal local strength $\sigma_{1,I}$ for each specimen necessary to define the linear law (Table 4).

The high values of the coefficient of variation are explained by large scatter inherent to natural materials, as is the case with bone. A coefficient of variation (CoV) around 30% is normal in such cases and, in this work, CoV = 36.5%-38.2% were obtained for the material parameters listed in Table 4, which is within the acceptable range. It should be noted that these high values of CoV can be avoided performing a large number of tests. This was not accomplished in this work, since the main goal was to present a suitable methodology to deal with mode I fracture characterisation of bone-cement connection.

6. Conclusions

Human beings suffer many traumatic injuries during their lifetime that reduces quality of life. Consequently, there is an immediate need to improve and develop new solutions for the stabilisation of bone fractures. The objective of this work focusses on the mechanical performance of bonded bone tissue connections using low viscosity orthopaedic bone cement to design efficient bonding systems. Double Cantilever Beam fracture tests were performed considering bone-PMMA cement bonded joints. The *Resistance*-curves (*R*-curves) were obtained from the load–displacement curves considering an equivalent crack length based procedure (i.e., the compliance based beam method, CBBM). The critical values of fracture energy under mode I loading (G_{Ic}) were defined from the plateau of those curves. A finite element numerical analysis including cohesive zone modelling was performed aiming to validate the followed procedure and to determine the cohesive law representative of the fracture behaviour of this bonded joint, considering an inverse procedure. The good agreement obtained between the numerical and experimental load–displacement and *R*-curves demonstrates the appropriateness of the followed procedure.

The low values of fracture energy obtained for this bonded connection highlights the need to increase the research on this topic. In fact, it would be interesting that these bone cements could have higher toughness values, envisaging increasing their application in the context of stabilisation systems of bone to heal fractures.

Ethical approval: Not required.

Author contribution

T.D. Campos: Methodology, Investigation, Writing – original draft. **M.L.S. Barbosa:** Methodology, Investigation, Writing – original draft. **A.A.R. Olmos:** Formal analysis. **M. Martins:** Software, Resources. **F.A.M. Pereira:** Software, Data curation. **M.F.S.F. de Moura:** Conceptualisation, Methodology, Validation, Writing – review & editing, Supervision, Funding acquisition. **A. Zille:** Conceptualisation, Methodology, Investigation, Writing – original draft. **N. Dourado:** Conceptualisation, Methodology, Validation, Writing – review & editing, Supervision, Funding acquisition.

Declaration of Competing Interest

The authors declare that they have no known competing financial interests or personal relationships that could have appeared to influence the work reported in this paper.

Acknowledgements

The first author acknowledges the Portuguese (FCT) for the conceded financial support through the reference grant PTDC/EME-SIS/28225/

2017. M.F.S.M. de Moura acknowledges the 'Laboratório Associado de Energia, Transportes e Aeronáutica' (LAETA) for the financial support by the project UID/EMS/50022/2020. The corresponding author acknowledges FCT for the conceded financial support through the reference projects PTDC/EME-SIS/28225/2017 and UID/EEA/04436/2019.

Funding: Portuguese Foundation for Science and Technology for MsC grant of the first author, and research project PTDC/EME-SIS/28225/2017.

References

[1] J.D. Heckman, R.W. Bucholz, P. Tornetta III, Rockwood and green's fractures in adults ISBN-13: (2015) 978–1605476773.
[2] J.-Y. Rho, L. Kuhn-Spearing, P. Zioupos, Mechanical properties and the hierarchical structure of bone, Med. Eng. Phys. 20 (2) (1998) 92–102.
[3] A. Completo, F. Fonseca, Fundamentos de Biomecânica Músculo-Esquelética e Ortopédica. Publindústria. ISBN-13: 9789898927491, 2011.
[4] T.L. Norman, D. Vashishth, D.B. Burr, Fracture toughness of human bone under tension, J. Biomech. 28 (3) (1995) 309–320.
[5] Q.D. Yang, B.N. Cox, R.K. Nalla, R.O. Ritchie, Re-evaluating the toughness of human cortical bone, Bone 38 (6) (2006) 878–887.
[6] J.J.L. Morais, M.F.S.F. de Moura, F.A.M. Pereira, J. Xavier, N. Dourado, M.I. R. Dias, J.M.T. Azevedo, The double cantilever beam test applied to mode I fracture characterization of cortical bone tissue, J. Mech. Behav. Biomed. Mater. 3 (6) (2010) 446–453.
[7] F.A.M. Pereira, J.J.L. Morais, M.F.S.F. de Moura, N. Dourado, M.I.R. Dias, Evaluation of bone cohesive laws using an inverse method applied to the DCB test, Eng. Fract. Mech. 96 (2012) 724–736.
[8] A.J. Starr, Fracture repair: successful advances, persistent problems, and the psychological burden of trauma, JBJS 90 (1) (2008) 132–137.
[9] T.F. Freire, T. Quinaz, A. Fertuzinhos, N.T. Quyền, M.F.S.M. de Moura, M. Martins, A. Zille, N. Dourado, Thermal, Mechanical and Chemical Analysis of Poly(vinyl alcohol) Multifilament and Braided Yarns, Polymers 13 (21) (2021) 3644, https://doi.org/10.3390/polym13213644.
[10] P. Jordão, A. Bahute, U. Fontoura, P. Marques, Técnicas de cimentação femoral, Rev. Port Ortop e Traumatol. 21 (4) (2013) 473–478.
[11] R. Vaishya, M. Chauhan, A. Vaish, Bone cement, J. Clin. Orthop. Trauma 4 (4) (2013) 157–163.
[12] S. Saha, S. Pal, Mechanical properties of bone cement: a review, J. Biomed. Mater. Res. 18 (4) (1984) 435–462.
[13] C. Frias, O. Frazão, S. Tavares, A. Vieira, A.T. Marques, J. Simões, Mechanical characterization of bone cement using fiber Bragg grating sensors, Mater. Des. 30 (5) (2009) 1841–1844.
[14] K.A. Mann, S. Bhashyam, Mixed-mode fracture toughness of the cobalt-chromium alloy/polymethylmethacrylate cement interface, J. Orthop. Res. 17 (1999) 321–328.
[15] K.A. Mann, R. Mocarski, L.A. Damron, M.J. Allen, D.C. Ayers, Mixed-mode failure response of the cement-bone interface, J. Orthop. Res. 19 (6) (2001) 1153–1161.
[16] X. Wang, C.M. Agrawal, A mixed mode fracture toughness test of bone-biomaterial interfaces, J. Biomed. Mater. Res. 53 (6) (2000) 664–672.
[17] D. Systèmes, S. Academic, Abaqus License Software, Providence, RI, USA, 2021.
[18] F.A.M. Pereira, M.F.S.F. de Moura, N. Dourado, J.J.L. Morais, F.G.A. Silva, M.I. R. Dias, Bone fracture characterization under mixed-mode I + II loading using the MMB test, Eng. Fract. Mech. 166 (2016) 151–163.
[19] J. Oliveira, M. Demoura, M. Silva, J. Morais, Numerical analysis of the MMB test for mixed-mode I/II wood fracture, Compos. Sci. Tecnol. 67 (9) (2007) 1764–1771.
[20] J.P.M. Gonçalves, M.F.S.F. de Moura, P.M.S.T. de Castro, A.T. Marques, Interface element including point-to-surface constraints for three-dimensional problems with damage propagation, Eng. Comput. 17 (1) (2000) 28–47.
[21] A. Turon, C.G. Dávila, P.P. Camanho, J. Costa, An engineering solution for mesh size effects in the simulation of delamination using cohesive zone models, Eng. Fract. Mech. 74 (10) (2007) 1665–1682.